Letter
Vol. 43, No. 21 / 1 November 2018 / *Optics Letters* 5283

Optics Letters

Alignment-free integration of apertures and nontransparent hulls into 3D-printed micro-optics

ANDREA TOULOUSE,[1,*] SIMON THIELE,[1] HARALD GIESSEN,[2] AND ALOIS M. HERKOMMER[1]

[1]Institute for Applied Optics (ITO) and Research Center SCoPE, University of Stuttgart, Pfaffenwaldring 9, 70569 Stuttgart, Germany
[2]4th Physics Institute and Research Center SCoPE, University of Stuttgart, Pfaffenwaldring 57, 70569 Stuttgart, Germany
*Corresponding author: toulouse@ito.uni-stuttgart.de

Received 14 August 2018; revised 30 September 2018; accepted 1 October 2018; posted 1 October 2018 (Doc. ID 341906); published 22 October 2018

The fabrication of 3D-printed micro-optical systems by femtosecond direct laser writing is state of the art. However, the inherent transparency of the lens mount, which is also made of photopolymer, causes a degradation of the image contrast due to stray light and scattering. Furthermore, apertures play a key role in optical design but cannot be directly integrated during 3D printing. Here, we present a superfine inkjet process for targeted filling of 3D-printed cavities in order to integrate apertures and nontransparent hulls without any alignment. Considerable contrast improvement and micro-optical systems with increased functionality are demonstrated.

https://doi.org/10.1364/OL.43.005283

The fabrication of 3D-printed microlenses and submicrometer structures using direct laser writing with a two-photon polymerization process (2PP-DLW) is state of the art [1–6]. Advances have been made in intensity-shaping optics such as functional and corrective phase elements [7,8], integrated mode sorters [9], or micro-optical structures on fibers [10–13]. In particular, in the field of 3D-printed high-quality imaging optics in the micrometer range and above, recent progress has drawn high attention [14–16]. Fields of application are, for instance, endoscopy or sensing. The imaging performance of these lenses is, however, insuperably limited with regards to image contrast in this all-transparent material system. The reasons are manifold: the most obvious and severe one is the direct influence of stray light that enters the lens system from the side as depicted schematically in Fig. 1A. Furthermore, the 3D-printed lens mounts potentially open parasitic light paths that lower the image contrast locally. Also, scattering and absorption in the bulk material and Fresnel losses at the surfaces lead to an altered light distribution. It is therefore crucial to minimize the number of lenses and establish a process for the realization of light-blocking structures.

There are various approaches for the fabrication of optical apertures on a micrometer scale. For instance, laser microdrilling could be employed but is a subtractive process and thus poses the need for a nontransparent material on the lens and additional alignment steps. Intransparent thin-film coating, e.g., by shadow evaporation deposition, comparable to Ref. [17] on a micrometer scale with targeted positioning of the spheres could be another approach but is not suitable for the fabrication of hulls or buried structures. Furthermore, multiple processes for the fabrication of adaptive wafer-level apertures have been demonstrated [18,19]. All these approaches, however, lack the possibility of one-step integration and autoadjustment of the aperture position.

A suitable approach for alignment-free aperture fabrication and contrast enhancement in the field of 3D-printed micro-optics has not been published to date to the authors' knowledge and will be presented in the following. Our proposed superfine inkjet process for the realization of apertures and nontransparent hulls both shields stray light and adds additional optical design parameters, namely diameter, shape, and position of the aperture. We use metallic nanoparticle inks that dry within a short time frame and can be annealed into solid films at temperatures below the polymer degradation threshold. Internal cavities can be filled with the nontransparent ink via microfluidic forces. The fabricated nontransparent structures are defined

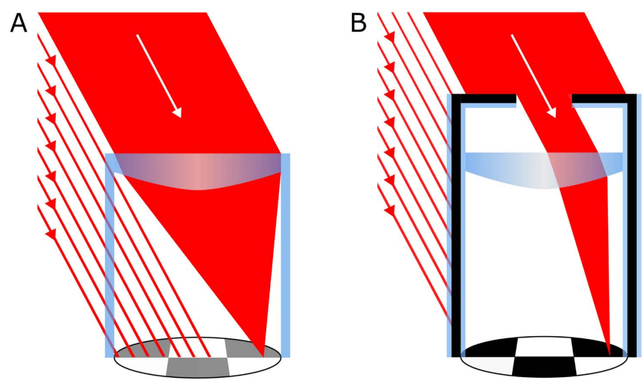

Fig. 1. Effects of a nontransparent aperture and hull. A, scheme of a transparent microlens, light field, stray light, and low-contrast image of a board pattern. B, scheme of a microlens with aperture and nontransparent hull under equivalent conditions with bended chief ray angle and high-contrast image.

0146-9592/18/215283-04 Journal

in the same 3D-printing step as the lens, and therefore no additional alignment is needed.

The optical designs presented in this work are simulated and optimized using the sequential mode of the commercial ray-tracing software ZEMAX and have a typical size of 300–400 μm in the z direction. The shape of the optimized lens is exported to the computer-aided design (CAD) software SolidWorks in order to add a lens mount, the physical aperture, and the microfluidic channels for the ink. Microfluidic channels and aperture basins feature a thickness on the order of 10–30 μm. The hull design comprises a cavity for the ink as well as holes for the development of the photo resist with acute angles to prevent the ink from pouring out of the designated volume due to its surface tension. For stray light analysis, this 3D model is reimported to the nonsequential mode of ZEMAX where the ink-filled structures are simulated as perfectly absorbing surfaces. Subsequently, the model is sliced, hatched, and finally fabricated by 3D dip-in 2PP-DLW using the Photonic Professional GT (Nanoscribe GmbH) and the proprietary photo resist IP-S [20] on a glass substrate with an ITO coating. The exposed samples are developed in mr-Dev 600 for up to 12 h and subsequently rinsed with isopropanol. The nontransparent structures are fabricated using an SIJTechnology, Inc. Super Inkjet Printer (Model SIJ-S030) that can dispense droplet volumes of 0.1 fl to 10 pl. A scheme of the inkjet process is depicted in Fig. 2. The ink utilized for the creation of the nontransparent structures is NPS-J (NANOPASTE series, Harimatec, Inc.), i.e., a conductive ink that comprises a silver nanoparticle content of 65 mass% with a particle size of 12 nm. The ink is pipetted into a hollow needle with a tip diameter of single micrometers that comprises an electrode and can be moved in z direction via a micrometer screw. The glass substrate with the 3D-printed microlens is placed onto the workstage that can be moved in steps of single micrometers in a range of several 10 mm in the x and y direction. Electric field pulses of 100–2000 V are applied in order to dispense ink droplets from the needle until the desired volume is completely filled.

The benefit of nontransparent structures in micro-optics can be demonstrated by the fabrication of selected optical systems with apertures and hulls as key design parameters, namely a micropinhole camera, an asphere with front aperture, and an image-space telecentric lens.

The first and most obvious demonstrator is a micropinhole camera (Fig. 3). A pinhole diameter of 27.7 μm is designed such that the pinhole resembles the first Fresnel zone on axis at a wavelength of 640 nm with a numerical aperture (NA) of 0.046. For qualification, the images of a micropinhole camera without ink and filled with ink are compared. We use a Thorlabs MCWHLP1 white light LED and beam-shaping optics for back illumination of a 50× Edmund Optics M Plan APO microscope objective with NA 0.55. The object (a negative USAF 1951 resolution test chart) is placed between the objective and sample and illuminated in transmission. The micropinhole camera is placed at a distance of approximately 10 mm from the object. The image plane of the micropinhole camera is recorded with an Edmund Optics video microscope setup consisting of a 20× M Plan APO objective with NA 0.42, an MT-4 tube lens with a focal length of 200 mm, and an IDS UI-3180CP-C-HQ Rev.2 camera. The camera is calibrated at a clear position on the sample with a white balance using the gray-world algorithm. The RGB image is converted to gray scale according to Rec.ITU-R BT.601-7 by forming the weighted sum $0.2989 \cdot R + 0.5870 \cdot G + 0.1140 \cdot B$ of the R, G, and B components. Exposure times are 3 ms for the transparent micropinhole camera and 60 ms for the blackened micropinhole camera. It is clearly visible that the image of the first is dominated by stray light at only 5% illumination time of the latter for which image formation is evident. The maximum contrast $K = (I_{\max} - I_{\min})/(I_{\max} + I_{\min})$ in Fig. 3E is 0.84 with a threshold of >100 counts for both minimum and maximum gray values $I_{\min}$ and $I_{\max}$.

As a second example, we extend the simple micropinhole camera with a single lens—inspired by the Wollaston landscape lens [21]—but optimize it with even aspherical terms to the 10th order, exploiting the design freedom of 3D printing (Fig. 4). Both the aperture and lens are optimized with sequential ray tracing for a maximum ratio of image size over spot size

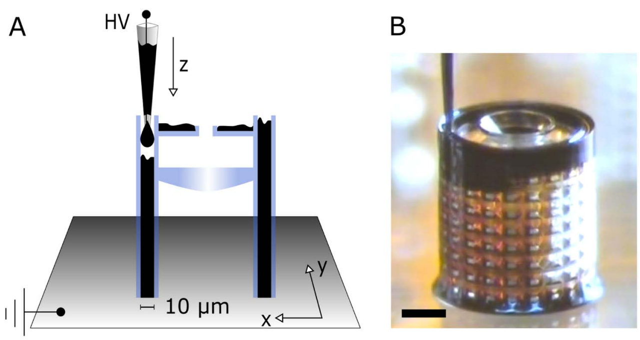

Fig. 2. Superfine inkjet process. A, scheme of the inkjet process. HV, high voltage pulses of 100–2000 V. B, microscope image taken during the inking process of a hull. Scale bar, 150 μm.

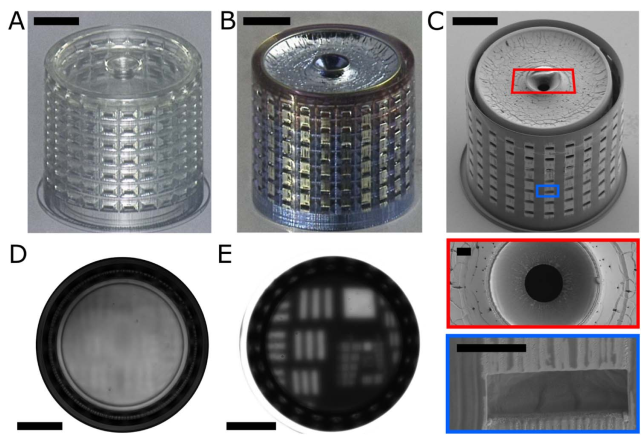

Fig. 3. Micropinhole camera. A, 3D-printed transparent micropinhole camera. B, 3D-printed micropinhole camera with aperture and nontransparent hull. C, SEM images of the micropinhole camera with aperture and nontransparent hull. Overview (top) and high-magnification images of the aperture and a hull feature (bottom, scale bars here are 10 μm). D, image of a USAF 1951 resolution test chart dominated by stray light in the focal plane of the all transparent pinhole camera (3 ms frame capture time). E, high-contrast image of a USAF 1951 resolution test chart in the focal plane of the pinhole camera with aperture and nontransparent hull (60 ms frame capture time). Scale bars, 100 μm.

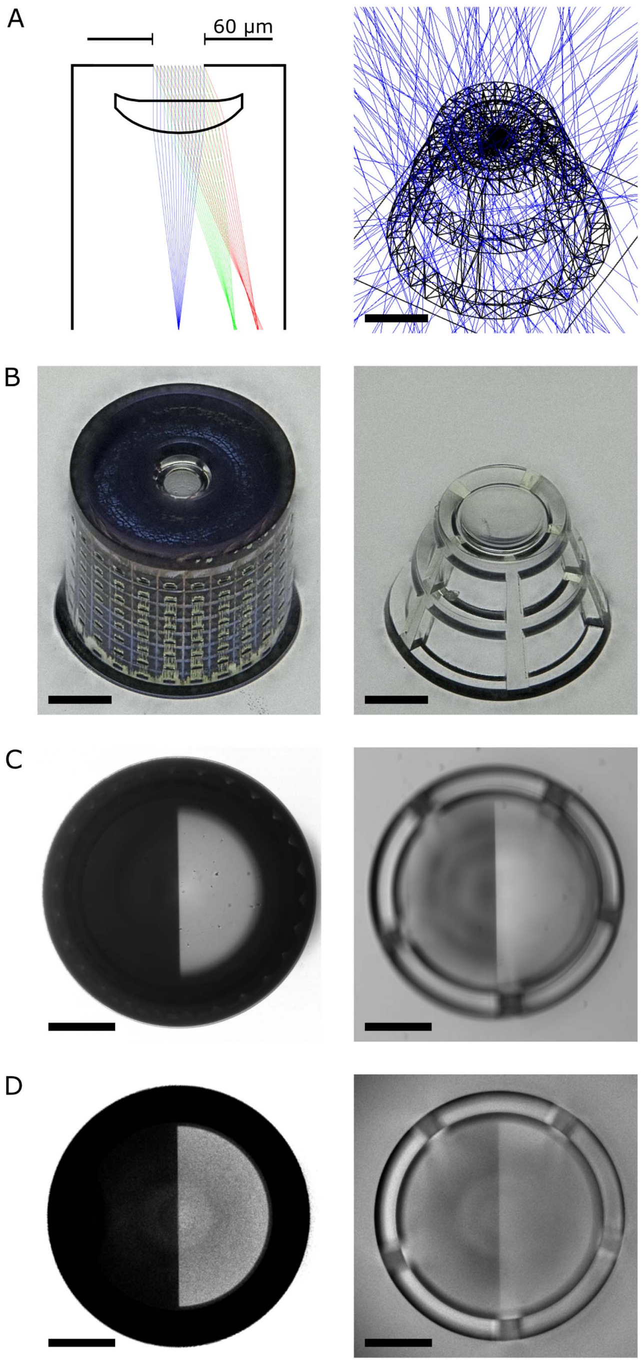

Fig. 4. Asphere with front aperture. A, optical design using sequential ray tracing (left) and nonsequential analysis of the transparent CAD design (right). B, 3D-printed asphere with front aperture and nontransparent hull (left) and 3D-printed asphere without aperture and hull (right). C, image of a razor blade in the focal plane of the asphere with (left) and without (right) nontransparent structures. D, nonsequential image simulation of a razor blade imaged by the asphere with (left) and without (right) nontransparent structures. Scale bars, 100 μm.

while assuring diffraction-limited performance [Fig. 4A(left)]. The lens is fabricated in a fully transparent version and with a nontransparent hull and aperture for comparison (Fig. 4B). We use a Thorlabs MCWHLP1 white light LED and a collimator to image the LED onto a diffusion disc to maintain a homogeneous illumination distribution for back illumination of a 50× Edmund Optics M Plan APO microscope objective with NA 0.55. A razor blade is placed between the objective and sample and illuminated in transmission. The microlens is placed at a distance of approximately 10 mm from the razor blade. The illumination time is 4 times higher for the lens with the nontransparent aperture and hull. The image of the microlens is recorded and processed as described above. As expected from the nonsequential image simulation [Figs. 4A (right) and 4D], the measurement proves a significant contrast improvement for the lens with nontransparent structures [Fig. 4C (left)] compared to the all-transparent lens [Fig. 4C (right)], namely from 0.44 to 0.76, respectively. The residual deviation from a perfect contrast can be explained by stray light caused by the transparent supportive structure at the rim of the aperture, stray light that enters the microscope objective from outside the microlens, irregularities, and scattering of the ink-filled structures, and luminescence of the photoresist. Apart from the contrast improvement, it is evident that the representation of dark structures, i.e., the image of the razor blade, is more homogeneous for the lens with the nontransparent aperture and hull. It can be concluded that, additionally to the contrast improvement, the transparent lens fixture is obscured successfully, whereas in the all-transparent case, the supportive structures lead to disruptive artifacts at the rim of the image plane.

Apertures and their positions play a key role for controlling telecentricity in optical design. Telecentricity is of interest for various applications. For instance, the microlens arrays on camera chips such as CMOS sensors typically have only high efficiency at small angles of incidence [22], and optical fiber bundles have strict limitations in terms of the chief ray angle. Here, we present an image-space telecentric design with a single aspherical lens and compare it to the same lens without aperture (Fig. 5). Both lenses are measured in the same setup as the micropinhole camera with a metal stripe of fixed width as an object and adapted exposure times. The image diameter at different z positions of the microlens is evaluated by determining the minimum and maximum profile gradient as depicted in Fig. 5B. A characteristic property of telecentricity is that chief rays of each field impinge on the image plane perpendicularly. The image magnification therefore does not change when the lens is defocused in a perfectly telecentric system. The image diameter is plotted over the z position (defocus) of the microlens in Fig. 5C. For the telecentric design, i.e., the design with aperture, a decrease in slope of 70% can be observed. The reason for the deviation from a perfectly telecentric design is assumed to be due to the shape fidelity of the lens surfaces, which is on the order of single micrometers and leads to a defocus and subsequent positioning error of the aperture with respect to the focal length. Generally in 3D printing, telecentricity can also be achieved without a nontransparent aperture but with multiple lenses. The clear advantage of an aperture instead is, however, the minimization of air–polymer transitions and the optical path in the polymer.

We demonstrated that superfine inkjet printing of metallic nanoparticle inks is a viable complementary approach for the integration of apertures and nontransparent hulls into 3D-printed micro-optics. The gain in design freedom for lens fixtures and the image quality improvement by contrast

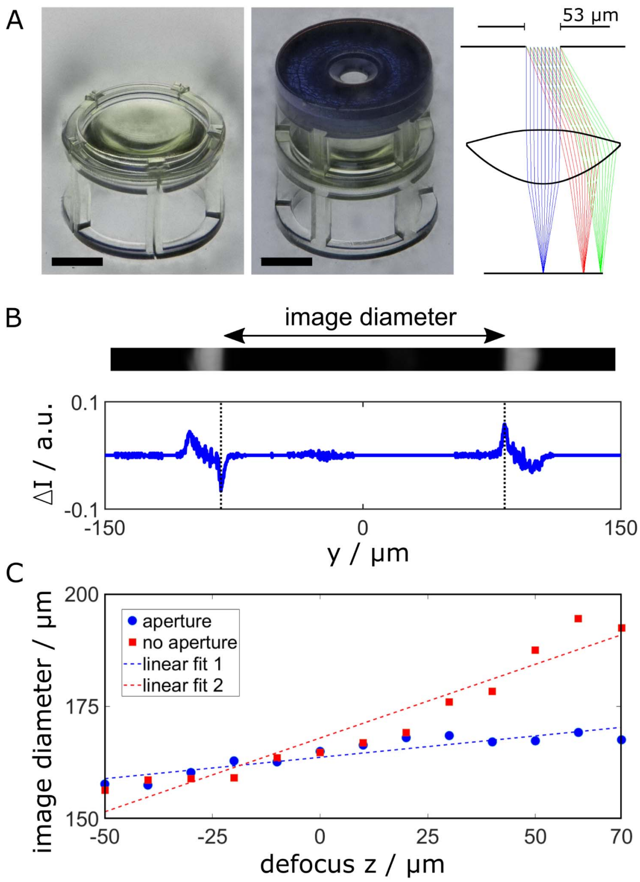

Fig. 5. Image-space telecentric lens. A, 3D-printed microlens without aperture (left), telecentric microlens with aperture (center), and telecentric optical design using sequential ray tracing (right). B, slice of the measured image of the metal stripe in focus of the telecentric design (top) and gradient of the intensity profile of the image (bottom). Dotted vertical lines at the minimum and maximum gradient, respectively. C, image diameter over z position (defocus) for the design without aperture and the telecentric design with aperture. Fit 1, diameter(μm) $= 0.095z + 164$ μm; fit 2, diameter(μm) $= 0.33z + 168$ μm. Scale bars, 100 μm.

enhancement are significant. Furthermore, this approach paves the way for the realization of a variety of micro-optical systems with alignment-free apertures in key positions, such as spectrometers or confocal systems. It is moreover a potential approach for the fabrication of smooth silver films to realize reflective surfaces for mirrors and catadioptric designs.

Funding. Bundesministerium für Bildung und Forschung (BMBF) (PRINTOPTICS, PRINTFUNCTION); Baden-Württemberg Stiftung (OPTERIAL); H2020 European Research Council (ERC) (ComplexPlas).

Acknowledgment. We thank the Baden-Württemberg Stiftung for filing this method as a patent (EP 3 162 549 A1).

REFERENCES

1. R. Guo, S. Xiao, X. Zhai, J. Li, A. Xia, and W. Huang, Opt. Express **14**, 810 (2006).
2. M. Malinauskas, H. Gilbergs, A. Žukauskas, V. Purlys, D. Paipulas, and R. Gadonas, J. Opt. **12**, 035204 (2010).
3. M. Malinauskas, A. Žukauskas, V. Purlys, K. Belazaras, A. Momot, D. Paipulas, R. Gadonas, A. Piskarskas, H. Gilbergs, A. Gaidukevičiūtė, I. Sakellari, M. Farsari, and S. Juodkazis, J. Opt. **12**, 124010 (2010).
4. M. Malinauskas, A. Žukauskas, K. Belazaras, K. Tikuišis, V. Purlys, R. Gadonas, and A. Piskarskas, Eur. Phys. J. Appl. Phys. **58**, 20501 (2012).
5. J. Fischer and M. Wegener, Laser Photon. Rev. **7**, 22 (2013).
6. S. Fischbach, A. Schlehahn, A. Thoma, N. Srocka, T. Gissibl, S. Ristok, S. Thiele, A. Kaganskiy, A. Strittmatter, T. Heindel, S. Rodt, A. Herkommer, H. Giessen, and S. Reitzenstein, ACS Photon. **4**, 1327 (2017).
7. S. Lightman, G. Hurvitz, R. Gvishi, and A. Arie, Appl. Opt. **56**, 9038 (2017).
8. A. Antonini, S. Bovetti, C. Moretti, F. Succol, V. P. Rajamanickam, A. Bertoncini, T. Fellin, and C. Liberale, in *European Quantum Electronics Conference* (Optical Society of America, 2017), p. 1.
9. S. Lightman, G. Hurvitz, R. Gvishi, and A. Arie, Optica **4**, 605 (2017).
10. G. Cojoc, C. Liberale, P. Candeloro, F. Gentile, G. Das, F. de Angelis, and E. Di Fabrizio, Microelectron. Eng. **87**, 876 (2010).
11. S. Bianchi, V. P. Rajamanickam, L. Ferrara, E. Di Fabrizio, C. Liberale, and R. Di Leonardo, Opt. Lett. **38**, 4935 (2013).
12. T. Gissibl, M. Schmid, and H. Giessen, Optica **3**, 448 (2016).
13. T. Gissibl, S. Thiele, A. Herkommer, and H. Giessen, Nat. Commun. **7**, 11763 (2016).
14. T. Gissibl, S. Thiele, A. Herkommer, and H. Giessen, Nat. Photonics **10**, 554 (2016).
15. S. Thiele, K. Arzenbacher, T. Gissibl, H. Giessen, and A. M. Herkommer, Sci. Adv. **3**, e1602655 (2017).
16. Z. Hong and R. Liang, Sci. Rep. **7**, 7145 (2017).
17. U. Håkanson, J. Persson, F. Persson, H. Svensson, L. Montelius, and M. K.-J. Johansson, Nanotechnology **14**, 675 (2003).
18. C.-H. Kim, K.-D. Jung, and W. Kim, in *IEEE 22nd International Conference on Micro Electro Mechanical Systems* (IEEE, 2009), pp. 156–159.
19. P. Müller, R. Feuerstein, and H. Zappe, J. Microelectromech. Syst. **21**, 1156 (2012).
20. T. Gissibl, S. Wagner, J. Sykora, M. Schmid, and H. Giessen, Opt. Mater. Express **7**, 2293 (2017).
21. K. Henney and B. Dudley, *Handbook of Photography* (Whittlesey House, McGraw-Hill, 1939).
22. P. B. Catrysse and B. A. Wandell, J. Opt. Soc. Am. A **19**, 1610 (2002).